

Azimuth and Slowness Deviations from the GERESS Regional Array

by Götz H. R. Bokelmann

Abstract For high signal-to-noise ratio events, body-wave travel times at GERESS stations are well fit by a plane-wave model corresponding to travel time uncertainties of about 1/100 sec. Slownesses obtained in this study are accurate to about 0.5 sec/deg, while azimuth uncertainties are about 2° for regional events and about 5° for teleseismic nuclear events. For illustration, we demonstrate performance for Nevada and Tuamotu nuclear tests and for regional events from Poland. Unbiased measurement requires array topography (about 200 m for GERESS) to be taken into account. If ignored, these elevation variations give rise to a systematic shift of about 0.6 sec/deg to eastern directions, which is almost independent of source location. In principle, arrays extending in vertical direction (“3D array”) can measure the vertical slowness and hence local material velocity c . For GERESS, we find $c \approx 5.2$ km/sec.

Compared with given accuracies, the regional GERESS array finds statistically significant deviations of slownesses and azimuths. These may be used to investigate lateral heterogeneity at regional scale.

Introduction

Seismological arrays are primarily important in the context of detection, location, and identification of seismic events. Their use was first proposed in the Geneva Conference in 1958, and since then, arrays have been installed in most regions around the world. Initially, the emphasis of this program was on arrays optimized to detect weak signals at teleseismic distances. The arrays satisfying this need were typically rather large in size, up to several hundred kilometers (LASA, NORSAR). More recently, within the negotiations toward a Comprehensive Test Ban Treaty, attention shifted to seismic detection at regional distances (up to 3000 km). Regional detection requires a different array design, optimized to detect phases propagating at regional distances. The new type of “regional array” is usually characterized by apertures of just a few kilometers. A prototype array is NORRESS in Southern Norway (Mykkeltveit *et al.*, 1990) with an aperture of about 3 km. Other examples are the associated arrays ARCESS and FINESA and the slightly larger GERESS array (Harjes, 1990).

Large amounts of data from both the older teleseismic arrays and the newer regional arrays are available; in this article, the latter type is discussed. Event location and identification at regional distances is usually a prime focus of array analysis, but these data are also applicable to the characterization of Earth’s heterogeneity.

In general, the distinguishing feature of arrays is the capability of measuring components of the slowness vector \mathbf{p} for individual seismological phases. Each component, p_x , of this vector represents the slowness (velocity⁻¹), dT/dx_x , in direction x_x . The length p_{\parallel} of the horizontal projection, called

“ray parameter” or horizontal slowness, directly represents the reciprocal velocity at the turning point of a ray in a 1D medium. While p_{\parallel} has been used extensively to infer average 1D Earth structure, the angle of the horizontal projection with the northern direction gives the back azimuth, which, in the absence of lateral heterogeneity, is the source-receiver great-circle direction. For events with known source locations, however, azimuth deviations of several degrees from the reference model are typical for most arrays. For different arrays, such anomalous effects were qualitatively ascribed to lateral heterogeneity in the lower mantle (Davies and Sheppard, 1973; Weichert, 1972), the crust and upper mantle (Berteussen, 1975; Faber *et al.*, 1986; Okal and Kuster, 1975), and a sedimentary layer under the respective array (Krüger and Weber, 1992).

Clearly, slowness data may contain important information about lateral heterogeneity of the Earth. Until very recently, however, there were no attempts to use azimuth and slowness information quantitatively, namely, in formal inversions. However, these quantities are particularly attractive for quantitative purposes, since they offer constraints on the Earth model that differ fundamentally from those given by travel times or amplitudes. In the ray-theoretical limit (Červený, 1987), the horizontal slowness vector has particular significance, since it is linearly related to lateral gradients of reciprocal velocity. The slowness vector also describes the kinematics of the ray. While essential characteristics of such inversions have been shown (Hu and Menke, 1992; Bokelmann, 1993), applications to data are rare. In preparing for such applications, we must first assess whether

observed slowness and azimuth values deviate significantly from reference model values. Particularly for smaller arrays, the measurement accuracies might be large enough to render observed slowness deviations insignificant.

Extracting (p_x, p_y, p_z) from waveform data is an inverse problem itself. In this article, the slowness estimation for a number of events with good signal-to-noise ratio is studied, using data from known source locations (nuclear events from Nevada and Tuamotu and regional mining-induced events from Poland) to eliminate mislocation uncertainty and the scatter from colocated events to check the uncertainty (accuracy). For these events, significant deviations can be attributed to lateral heterogeneity. The question of slowness accuracy is closely related to the achievable source-location accuracy and is therefore of interest also for characterizing source-location capability.

In addition to the slowness vector components estimated using array data, particle motion polarizations from three-component instrument data also permit an estimate of the back-azimuth θ (Harris, 1990). In our experience, their associated measurement accuracy is quite good too (about 4°), given events with good signal-to-noise ratio. However, the polarization vector may systematically deviate from the slowness vector due to anisotropy and the free surface. This is extensively discussed in Bokelmann (1995); therefore, three-component data will not be considered in this article.

The GERESS Array

The German experimental seismic system (GERESS) (Harjes, 1990), shown in Figure 1, is a regional array with an aperture of about 4 km. In this article, data from 25 stations with 1 Hz vertical short-period instruments are used, sampled at 40 Hz (solid circles). Five stations also have colocated short-period three-component instruments, in one case with an additional broadband three-component instrument. The array is located in Eastern Bavaria, Germany, in a hilly region on a granitic outcrop of the Bohemian massive (A0 is located at $13^\circ 42' 07''$ E and $48^\circ 50' 12''$ N). The topographic variation across the array is about 200 m.

Figure 2 shows a waveform example (event 6 of Table 1) recorded on the 25 vertical component stations of the GERESS array, a French nuclear explosion on Fangataufa on the Tuamotu Archipelago, South Pacific, at 154° distance. To better illustrate the high spatial coherence of the data, time shifts across the array have been corrected. Particularly the first 2 sec of the waveform show good spatial correlation.

Travel Times and Slownesses

The standard method for estimating slowness vector components from such array data is the wavenumber spectrum technique, which is often used in automatic procedures (Fyen, 1987; Harjes *et al.*, 1993). This technique uses the full waveform information explicitly. However, extraction of the slowness vector can be demonstrated more easily us-

GERESS Array and Smoothed Topography

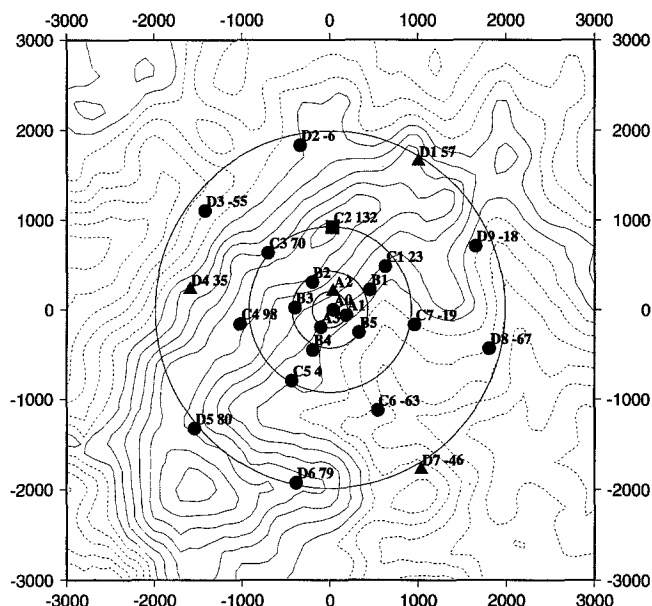


Figure 1. Station locations and elevations (labels) of the GERESS array in Southeastern Germany in meters. Filled circles show the 25 vertical short-period instruments used in this article, and the triangles and rectangles show the three-component instruments. Topographic variation across the array of about 200 m is shown by contour lines (increment of 25 m), with dashed lines for elevations below 1000 m. The number after the station name gives instrument elevation (located in vaults) relative to 1000 m, the first solid contour.

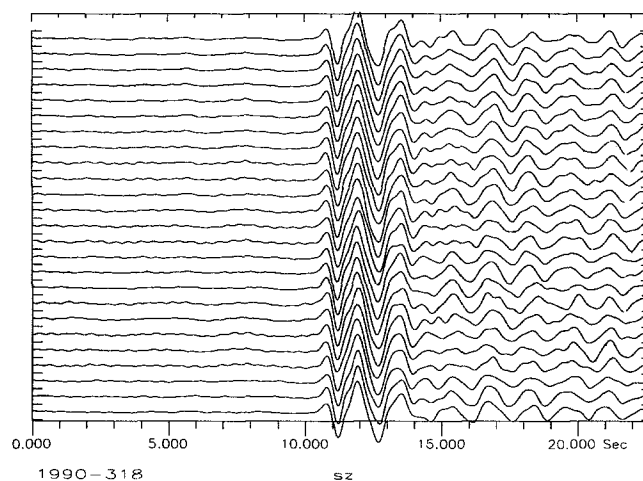


Figure 2. Waveform data from a French nuclear test on Fangataufa, Tuamotu, South Pacific (event 6 in Table 1; bandpass at 0.1 and 2.5 Hz). Time shifts across the array were corrected to illustrate the good coherence of the PKP waveform. For this example, the mean time residual after plane-wave fitting is 0.01 sec, well below the sampling interval of 0.025 sec.

Table 1
Events Used in This Study (Known Source Locations)

Number	Year:Day	Time	Latitude	Longitude	Mag.	Location	Phase	p_x /(sec/deg)	p_y /(sec/deg)
Teleseismic events									
1	1990:285	17.30.00.08*	37.26° N*	116.48° W*	5.6*	Nevada	P	-3.06 ± 0.49	3.78 ± 0.45
2	1991:094	19.00.00.0**	37.296° N**	116.313° W**	5.6**	Nevada	P	-2.80 ± 0.44	3.55 ± 0.34
3	1991:257	19.00.00.05**	37.226° N**	116.428° W**	5.5**	Nevada	P	-2.70 ± 0.26	3.49 ± 0.22
4	1991:291	19.12.00.00**	37.063° N**	116.045° W**	5.2**	Nevada	P	-2.95 ± 0.43	3.31 ± 0.37
5	1990:153	17.29.59.0*	21.82° S*	138.94° W*	5.3*	Mururoa†	PKP	-2.09 ± 0.56	2.18 ± 0.43
6	1990:318	18.11.58.4*	22.20° S*	138.84° W*	5.6*	Fangataufa†	PKP	-2.16 ± 0.35	2.45 ± 0.27
7	1990:325	16.59.58.4*	21.90° S*	138.98° W*	5.4*	Mururoa†	PKP	-2.00 ± 0.26	2.43 ± 0.20
8	1991:138	17.14.58.53**	21.832° S**	139.014° W**	5.1**	Mururoa†	PKP	-1.76 ± 0.23	2.56 ± 0.21
9	1991:149	18.59.58.24**	22.256° S**	138.794° W**	5.5**	Fangataufa†	PKP	-1.98 ± 0.29	2.67 ± 0.25
10	1991:165	17.59.57.86**	21.944° S**	138.988° W**	5.2**	Mururoa†	PKP	-1.77 ± 0.29	2.18 ± 0.25
11	1991:196	18.09.58.33**	21.877° S**	138.963° W**	5.3**	Mururoa†	PKP	-1.61 ± 0.38	2.02 ± 0.45
Regional events									
12	1991:059	15.29.40††	51.426° N††	16.243° E††	3.7‡‡	Poland	Pn	6.07 ± 0.46	11.65 ± 0.34
13	1991:120	03.40.36††	51.409° N††	16.264° E††	3.4‡	Poland	Pn	5.69 ± 0.27	11.61 ± 0.21
14	1991:143	19.42.54††	51.428° N††	16.242° E††	4.0‡‡	Poland	Pn	5.08 ± 0.64	10.49 ± 0.63
15	1991:191	23.57.16††	51.424° N††	16.217° E††	3.3‡	Poland	Pn	6.20 ± 0.26	11.26 ± 0.29
16	1991:222	05.23.48††	51.428° N††	16.242° E††	3.9††	Poland	Pn	6.55 ± 0.60	11.22 ± 0.53
17	1991:252	18.36.57††	51.414° N††	16.220° E††		Poland	Pn	6.36 ± 0.24	10.99 ± 0.21
18	1991:327	01.06.20††	51.428° N††	16.243° E††	3.9§	Poland	Pn	6.72 ± 0.40	11.14 ± 0.29

*ISC (mb). **PDE (mb). †DSIR. ††POL. ‡KRA (mL). ‡‡VKA (mL). §GRF (mL).

ing the simpler approach of extracting travel times \tilde{t}_i from the waveforms and fitting predicted times of a plane wave,

$$\tilde{t}_i = t_0 - \mathbf{p} \cdot \mathbf{r}_i, \quad (1)$$

to these. This is a linear inverse problem for the reference station time t_0 and the slowness vector $\mathbf{p} = (p_x, p_y, p_z)$, here defined positive from station to source. The term \mathbf{r}_i is the location vector of the i th station, including its elevation. For the high signal-to-noise ratio events in this study, we expect that the results will not differ significantly from the results of the wavenumber spectrum technique.

We tested different criteria for travel time extraction on a large number of events, based on either a fixed position in the waveform (onset, maximum, minimum, zero crossing) or by correlating parts of the waveform (cross-correlation, visual correlation). Using the interactive travel time picking facility of the RONAPP software package (Fyen, 1987) and subsequent plane-wave fitting, we find smallest residuals for cross-correlation methods. Compared with the cross-correlation method, visual correlation offers added flexibility in choosing window lengths. Selecting the main common feature in the first second of the raw waveform data used for Figure 2, we obtained a mean time residual of 0.01 sec. Note that this mean residual implies accuracies substantially better than the sampling interval of 0.025 sec. That is consistent with formal uncertainties for cross-correlations (Bokelmann, 1992), which can reach values of one-tenth of a sample interval depending on the signal-to-noise ratio. For good signal-to-noise ratio, the sampling rate is not the limiting factor, but waveform distortions (e.g., from noise contamination or

from physical effects), such as scattering from near-receiver heterogeneity, are the limiting factor. Further discussions of travel time extraction are found in Weichert (1975).

Uncertainties of p from SVD

Equation (1) describes a “forward” problem $\mathbf{t} = \mathbf{A}\mathbf{x}$ with model parameters $\mathbf{x} = (t_0, p_x, p_y, p_z)^T$. Using the singular value decomposition $\mathbf{A} = \mathbf{U}\mathbf{A}\mathbf{V}^T$, an estimate of the model vector is $\mathbf{x} = \mathbf{V}\mathbf{A}^{-1}\mathbf{U}^T\mathbf{t}$ (Menke, 1984), where \mathbf{A} is a diagonal matrix containing the singular values. This approach is not equivalent to the static corrections approach. The latter solves for p_x and p_y and approximates the effect of topography by accounting for delays along a vertical path only. The static corrections approach is an approximation for arrays with extent much larger in the horizontal than in the vertical direction. Correctly, that approach would require the incidence angle to be known. Otherwise, it poses a nonlinear inverse problem. The simple approach of equation (1), on the other hand, does not involve any approximations of that kind. In our linear problem, we can identify the contribution of the individual singular values. An example is shown in Table 2, which contains the singular values and the columns of the eigenmatrix \mathbf{V} for the travel times of the event in Figure 2. We see that three of the four singular values are of the same order of magnitude, but the fourth is an order of magnitude smaller. The eigenvector for that last singular value describes the influence of only the vertical slowness p_z on the data. This general feature, which occurs for all events in the study, is a reflection of the fact that p_z is more difficult to resolve than the other parameters, since it contributes an order of magnitude less to the data, since eleva-

Table 2
Singular Values and Right Eigenvectors of A

Singular Value nr Singular Value	1	2	3	4
	5.465	3.371	2.351	0.189
Eigenvector nr	1	2	3	4
t_0	-0.564	0.363	-0.734	0.102
p_x	0.0272	0.904	0.425	-0.008
p_y	-0.821	-0.222	0.524	0.020
p_z	-0.075	0.025	-0.067	-0.994

tion variations across the array are an order of magnitude smaller than the array aperture.

The solution \mathbf{x} depends on the number of singular values λ_j (diagonal elements of Λ) included in the inversion. Generally, the fit to the data \mathbf{t} improves when more singular values are included. Also, the resolution of individual model parameters \mathbf{x} increases. On the other hand, the model covariance matrix

$$\mathbf{C} = \mathbf{V}\Lambda^{-2}\mathbf{V}^T \quad (2)$$

shows generally increased variance for the model parameters, if small singular values λ_j are incorporated in the solution. This is the well-known trade-off problem between resolution and variance, which is typically studied for the decision of whether certain model parameters are included in the inversion. Before we address the question of whether p_z should be included in the inversion to improve the determination of p_x and p_y , we study implications of p_z itself. Given p_x , p_y , and p_z , we can directly compute the local propagation velocity $c = 1/\sqrt{p_x^2 + p_y^2 + p_z^2}$. This local velocity can, in principle, be constrained from a single good event, in which all three slowness vector components are constrained. This does not even require knowledge of the source location. Figure 3 shows a histogram of c estimates for first arrivals from a larger set of 108 events covering all azimuth and distance ranges. These values scatter considerably around the peak, which is at $c = 5.2$ km/sec. The histogram is not well fit by the standard Gaussian curve, but a distribution consisting of two added Gaussians with parameters $c_1 = 5.2 \pm 0.15$ km/sec and $c_2 = 5.7 \pm 1.5$ km/sec fits the data, suggesting two different populations. Surprisingly, for a subset of the events, apparently with favorable conditions, we obtain the estimate $c = 5.2$ km/sec with very tight bounds, but the uncertainty for the majority of the events is better characterized by the standard deviation $\sigma = 1.5$ km/sec. What distinguishes the subset with tighter distribution from the larger one is not clear. A few outliers can be identified as associated with large uncertainty and/or unphysical results (positive p_z).

The peak value of $c = 5.2$ km/sec is a rather reasonable value for the array, since it should represent an average velocity for the array subsurface (fresh and weathered granite, gneiss). This obtained value is the appropriate choice, for example, when converting from slowness $p_{||}$ to incidence an-

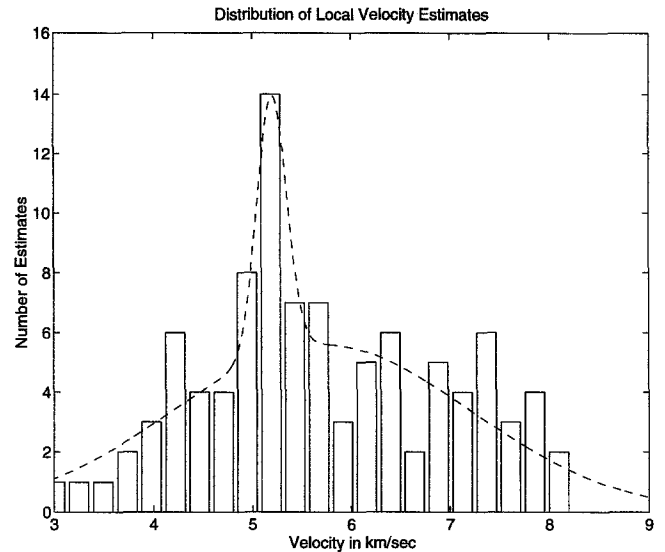


Figure 3. Histogram of local velocity estimates $c = 1/\sqrt{p_x^2 + p_y^2 + p_z^2}$ from a larger set of 108 regional and teleseismic events. The peak value is at 5.2 km/sec.

gle $\sin^{-1}(cp_{||})$. The waveform data (Table 1), discussed in the following section, contain regional and teleseismic events with apparent velocity ranging from 8 to 30 km/sec. Although the two signal types differ substantially in apparent velocity, the distributions for c are indistinguishable.

Slowness Estimates and Bias

Does accounting for p_z improve estimates of p_x and p_y ? Instead of deciding ad hoc whether to include p_z in the inversion, we compare results for both cases in the following section. Table 1 gives origin time, location, body-wave or local magnitude, and estimates of horizontal slownesses of 18 events, which are used in the following to discuss slowness estimation capability. Information for the teleseismic events is from ISC, PDE, and the Department for Scientific and Industrial Research (DSIR), New Zealand. For the regional events, the location information is from the Polish Bulletin, and magnitude estimates are from individual stations at Krakow (KRA), Vienna (VKA), and Gräfenberg (GRF).

Teleseismic Events

Events 1 through 4 in Table 1 are U.S. nuclear tests detonated in Southern Nevada; events 5 through 11 are French tests from the South Pacific. Slowness components p_x and p_y are shown in Figure 4a for the two regions with individual error bars indicating one standard deviation. These results are from an inversion for the four parameters (t_0, p_x, p_y, p_z), thereby accounting for array topography. Note that for each region the (p_x, p_y) estimates cluster tightly and that nearly all of the confidence regions overlap. While the theoretical back azimuth of 322.1° (line) is within the spread

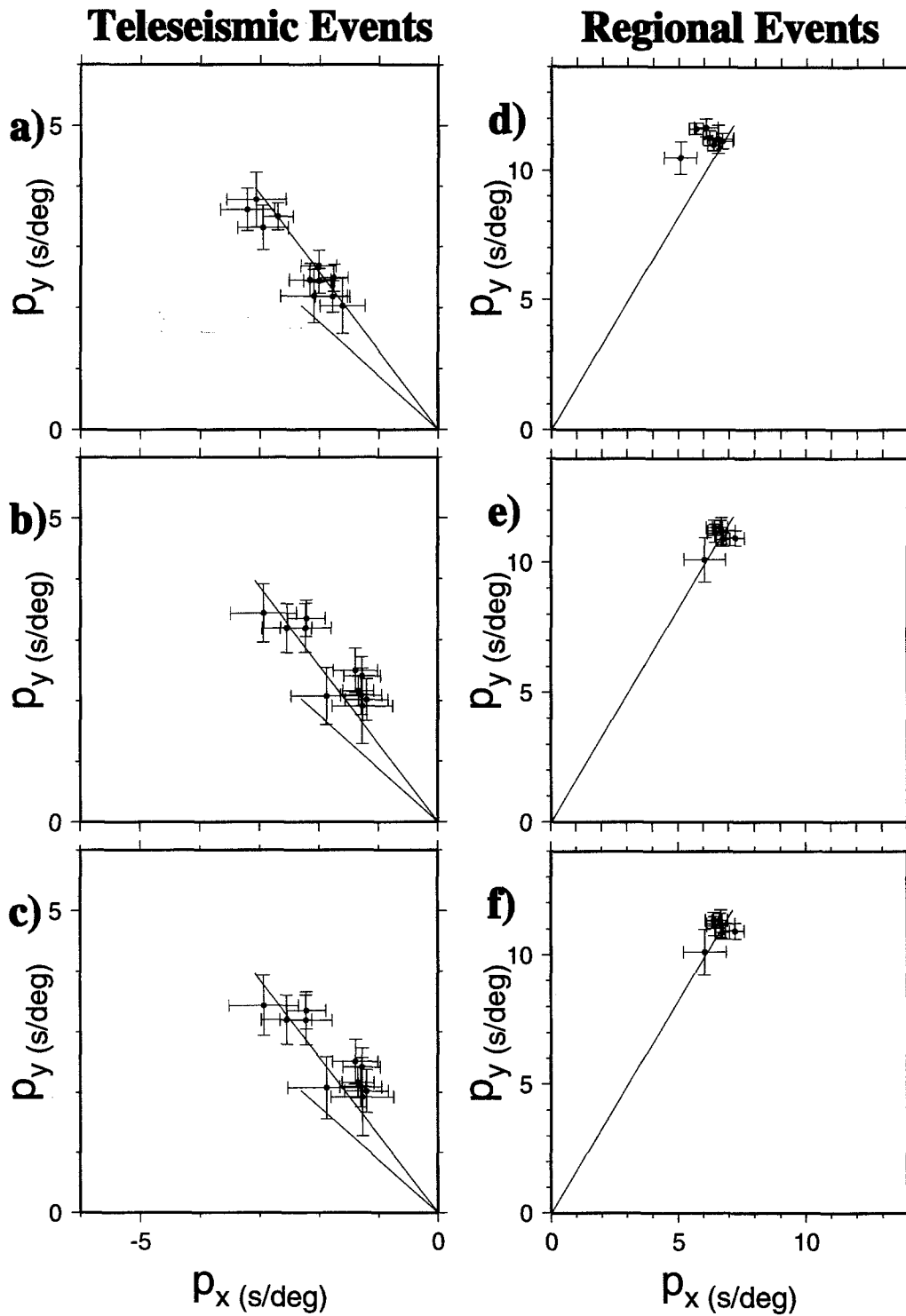


Figure 4. Results for the horizontal slownesses (p_x , p_y) in sec/deg for ((a) through (c)) teleseismic events (1 through 11 in Table 1) on the left and ((d) through (f)) regional events (12 through 18 in Table 1) on the right. The results on the top ((a) and (d)) are from inverting for (t_0, p_x, p_y, p_z) . Significant deviations from theoretical predictions are found for all three source regions, with the strongest effect being the clear azimuth offset of about 9° for the South Pacific events. The middle row ((b) and (e)) shows results from inversion for (t_0, p_x, p_y) , ignoring topography. The estimates are displaced to the southeast, which shows the bias from ignoring topography. The bottom row ((c) and (f)) is from restricting the full inversion to three singular values, with results very similar to the middle row. The omitted fourth singular value almost completely described the effect of p_z .

Table 3
Mean Azimuth and Slowness Deviation for Each Source Region

Region	Pred. θ	Obs. Mean $\bar{\theta}_{\text{obs}}$	Pred. p_{\parallel}	Obs. Mean $\bar{p}_{\parallel\text{obs}}$	$\frac{ \theta - \bar{\theta}_{\text{obs}} ^{*}}{\sigma_{\theta}}$	$\frac{ p_{\parallel} - \bar{p}_{\parallel\text{obs}} ^{*}}{\sigma_{p_{\parallel}}}$
Nevada	322.1°	320.8° ± 1.8°	5.13 sec/deg	4.56 sec/deg ± 0.21 sec/deg	0.7	2.7
Tuamotu	310.7°	320.9° ± 3.0°	3.13 sec/deg	3.04 sec/deg ± 0.26 sec/deg	3.4	0.3
Poland	31.7°	28.5° ± 2.1°	13.75 sec/deg	12.75 sec/deg ± 0.50 sec/deg	1.5	2.0

*Significant deviations of azimuth and slowness (larger than the scatter σ) are shown in boldface.

of observed azimuths for Nevada (distance 83°) of 318° to 322°, the predicted horizontal slowness $p_{\parallel} = 5.13$ sec/deg (for IASP91-model of Kennett and Engdahl, 1991) is not located within the range of observed values of 4.41 to 4.86 sec/deg. Table 1 gives average azimuth and slowness for the Nevada events as $320.8^{\circ} \pm 1.8^{\circ}$ and 4.56 sec/deg ± 0.21 sec/deg. Compared with predicted values, this suggests a statistically significant deviation in slowness, but not in azimuth. For the Tuamotu Archipelago events, back azimuths are in the interval 316° to 326° and deviate clearly from the predicted back azimuth of about 311°. Table 3 indicates that this azimuth deviation is significant at 3.4 σ , while the slowness deviation is not. While the Nevada events experience a significant slowness deviation, the Tuamotu events experience significant azimuth deviation. This indicates that the deviations cannot be caused by systematic biases of the inversion procedure but are true effects of lateral heterogeneity.

Figure 4b shows the results from inversion for (t_0, p_x, p_y) , which ignores topographic variation across the array. The standard deviations of p_x and p_y are about the same size as before, but the estimates of p_x and p_y show a bias: they are displaced systematically to the southeast. If we truncate the full inversion at three singular values, we obtain Figure 4c, which is essentially the same as Figure 4b. This is expected, since the previous discussion (Table 2) showed that the smallest singular value, which is omitted here, controls almost exclusively the contribution of p_z .

Regional Events

Now we inspect similarly (p_x, p_y) estimates for regional data. Events 12 to 18 in Table 1 are a set of regional events from Poland, all of which are mining-induced events from the same source area Rudno at distance 340 km. Error bars for individual slowness component estimates vary between 0.2 to 0.6 sec/deg, which is comparable to those for the teleseismic events in Figures 4a through 4c. Also for these regional events, estimates of p_x and p_y (Fig. 4d) deviate from predicted values, in azimuth but particularly in slowness. This is an effect that has previously been observed by Schweitzer (1992, personal comm.). Table 3 shows that both the observed azimuth and slowness deviations are significant. The scatter of azimuth and slowness estimates in Table 3 is comparable to formal errors obtained for individual events, suggesting that the error procedure of the inversions

is not only internally consistent but also gives us appropriate uncertainties. There is one outlier with large error bars (event 14). Since it appears in all inversions, it is not a feature of the inversion method but of the data set. Such large apparent uncertainty is suspect if sufficient care was taken in determining the travel times. In this case, the error may be caused by timing errors during the early stage of deployment of the array. Formal errors, in fact, are an excellent tool for quality control of the data. Figures 4e and 4f show deviations from the result of the full inversion, similar to the teleseismic examples.

Testing the Topographic Effect

We can test whether topography causes the different results of the full and the (p_x, p_y) -only inversions in Figure 4, by predicting the pattern for synthetic data, assuming a local velocity of 5.2 km/sec. For a set of regularly spaced events, Figure 5 gives the effect of ignored topography on p_x and p_y (slowness window of the teleseismic example of Fig. 4). The maximum effect at steep incidence is a shift of about 0.6 sec/deg in southeastern direction (106°), which corresponds well with the differences in Figure 4. The elevations in Figure 1 show that the prominent topographic feature is a ridge crossing the center of the array from SW to NE. Also, the SE is at lower elevation than the NW. This asymmetry induces the observed pattern of Figure 5. The arrows are essentially perpendicular to the direction of the topographic ridge on Figure 1. Their eastward direction is an effect of the elevation difference between NW and SE. Ignoring topography, an average plane wavefront fit to the travel times is therefore tilted to the west, causing the artificial eastern component of the horizontal slowness. The regularity of the pattern results from averaging over the whole array for each event. For larger slownesses, the effect slowly decreases and scatters in azimuth.

Discussion

In this article, we tested the slowness estimation capability of regional arrays and found that estimates of p_x and p_y can be fairly accurate, with mean uncertainties in this study of 0.35 sec/deg. These uncertainties can be seen as typical for scientific studies, where events with high signal-to-noise ratio are carefully processed. They are associated

Topographic Effect on Slowness Vector

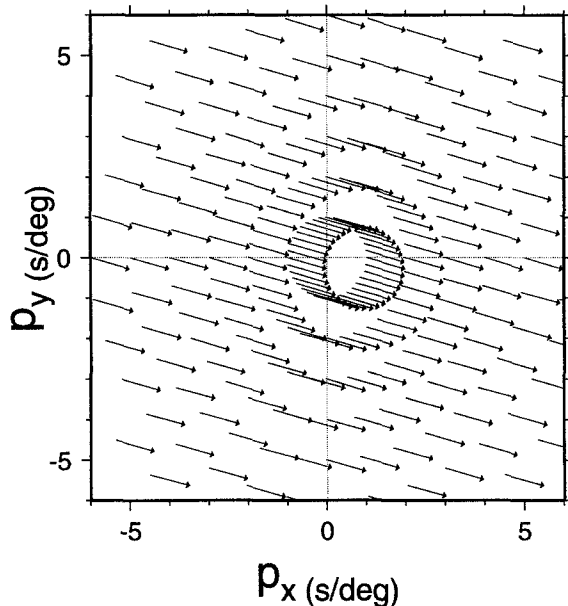


Figure 5. The effect of (ignored) GERESS topography on slowness vector estimates, a shift to the southeast ($\approx 106^\circ$) of up to 0.6 sec/deg, almost independent of the source location. For larger slowness, the effect decreases, and angles of the shift scatter.

with slowness uncertainties of 0.5 sec/deg. Azimuthal uncertainties depend on epicentral distance and are about 2° for regional events and 5° for teleseismic events.

We established that array mislocation effects from several source regions are significant. The strongest effect in this study occurs for Tuamotu events, with back azimuths deviating by about 10° to more northern directions. Events from Nevada and Poland give rise to smaller anomalies; however, their slowness deviations are also significant, even at the 2σ level. Although paths under the receivers are similar for events from Nevada and Tuamotu, they are perturbed differently: slowness deviations for Nevada and azimuth deviations for Tuamotu. Since such different behavior is difficult to explain by lateral heterogeneity under the receivers alone, distant heterogeneity is apparently involved. There are in fact stronger azimuth deviations than those presented in this article. However, the chosen set of events is not affected by source mislocation and is therefore ideally suited for our study of slowness estimation capability.

These results are encouraging the use of regional arrays for characterizing Earth's heterogeneity. Of course, the characteristic deviations in these data may also be used to remove certain biases from regional source locations, such as the biases from lateral heterogeneity and array topography. For events in this study, both effects are about the same size. We showed that ignoring topography, or correspondingly the vertical slowness, introduces artificial array mislocation ef-

fects for all three regions, which amounts to a shift in approximately southeastern direction of up to 0.6 sec/deg. Accounting for elevation changes, GERESS acts as a 3D array and supplies a direct estimate of the local velocity under the array, which is 5.2 km/sec.

Acknowledgments

The work of the GERESS group at Bochum is acknowledged, which is supported by ARPA grant AFOSR-90-0189. I profited from discussions with Johannes Schweitzer, Jan Wüster, and particularly, Hans-Peter Harjes, who also read the manuscript. Assistance in computation is acknowledged by Michael Jost and Nikolai Gester mann. Last but not least, I wish to thank two anonymous reviewers and Chuck Ammon for comments that substantially improved the clarity of the text.

References

- Berteussen, K. A. (1975). Array analysis of lateral inhomogeneities in the deep mantle, *Earth Planet. Sci. Lett.* **28**, 212–216.
- Bokelmann, G. H. R. (1992). Upper and lower mantle small-scale heterogeneity studied by systematic analysis of portable broadband waveforms and travel-times, *Ph.D. Thesis*, Princeton University, Princeton, New Jersey.
- Bokelmann, G. H. R. (1993). Array tomography for body waves: Inversion of travel times and ray parameters, *Annal. Geophys.* Part I, C-47.
- Bokelmann, G. H. R. (1995). P-wave array polarization analysis and effective anisotropy of the brittle crust, *Geophys. J. Int.* **120**, 145–162.
- Červený, V. (1987). Ray tracing algorithms in three-dimensional laterally varying layered structures, in *Seismic Tomography*, G. Nolet (Editor), D. Reidel Publishing Co., Dordrecht, Holland.
- Davies, D. and R. M. Sheppard (1973). Evidence for lateral heterogeneity in the Earth's mantle, *Nature* **239**, 318–322.
- Faber, S., J. Plomerová, and V. Babuska (1986). Deep-seated lateral velocity variations beneath the GRF array inferred from mislocation patterns and P residuals, *J. Geophys.* **60**, 139–148.
- Fyen, J. (1987). Improvements and modifications, Semiannual Technical Summary 1 October 1986–31 March 1987, NORSAR Sci. Rep. No. 2-86/87, Kjeller, Norway.
- Harjes, H. P. (1990). Design and siting of a new regional array in central Europe, *Bull. Seism. Soc. Am.* **80**, Part B, 1801–1817.
- Harjes, H. P., M. L. Jost, J. Schweitzer, and N. Gester mann (1993). Automatic seismogram analysis at GERESS, *Comput. Geosci.* **19**, Part 2, 157–166.
- Harris, D. B. (1990). A comparison of the direction estimation performance of high-frequency seismic arrays and three-component stations, *Bull. Seism. Soc. Am.* **80**, Part B, 1951–1968.
- Hu, G. and W. Menke (1992). Formal inversion of laterally heterogeneous structure from P-wave polarization data, *Geophys. J. Int.* **110**, 63–69.
- Kennett, B. L. N. and E. R. Engdahl (1991). Travel times for global earthquake location and phase identification, *Geophys. J. Int.* **105**, 429–465.
- Krüger, F. and M. Weber (1992). The effect of low-velocity sediments on the mislocation vectors of the GRF array, *Geophys. J. Int.* **108**, 387–393.
- Menke, W. (1984). *Geophysical Data Analysis: Discrete Inverse Theory*, Academic Press, London.
- Mykkeltveit, S., F. Ringdal, T. Kvaerna, and R. W. Alewine (1990). Application of regional arrays in seismic verification research, *Bull. Seism. Soc. Am.*, **80**, Part 6, 1777–1800.
- Okal, E. and G. Kuster (1975). A teleseismic array study in French Polynesia; implications for distant and local structure, *Geophys. Res. Lett.* **2**, Part 1, 5–8.

- Weichert, D. H. (1972). Anomalous azimuths of P: evidence for lateral variations in the deep mantle, *Earth Planet. Sci. Lett.* **17**, 181–188.
- Weichert, D. H. (1975). The role of medium aperture arrays: the Yellowknife system, in *Exploitation of Seismograph Networks*, K. G. Beauchamp (Editor), Nordhoff International, Leiden.

Institute of Geophysics
Ruhr-University Bochum
44780 Bochum, Federal Republic of Germany

Manuscript received 18 August 1993.